tion in degrees 2θ of the 131 and $1\bar{3}1$ lines depends strongly on the value of γ, and varies by 0.3° 2θ for $CuK\alpha$ radiation in the samples studied. When the compositions of the feldspars in Table 1 are known independently, the $131\text{-}1\bar{3}1$ separations given in Table 1 can be calibrated and may then prove useful in estimating feldspar compositions in other similar samples.

The cell parameters of calcic plagioclases vary slightly with change of composition and with Al/Si order. From investigations utilizing methods based on the indices of refraction (*6*) and on cell parameters and line positions (*7*) of terrestrial plagioclases, it appears that the lunar plagioclases in type B rocks are from 5 to 10 percent by weight more calcic than those in type A rocks, but that within each rock type the plagioclase composition varies relatively little. The lunar plagioclases do not differ in any obvious ways from terrestrial plagioclases that are chemically equivalent. If the compositional estimates in Table 1 are accurate, values of the parameters Γ and B (*7*) suggest that the plagioclases in type B rocks probably have relatively high Al/Si disorder compared to those in terrestrial intrusive igneous rocks.

DAVID B. STEWART
DANIEL E. APPLEMAN
J. STEPHEN HUEBNER
JOAN R. CLARK
U.S. Geological Survey,
Washington, D.C. 20242

References and Notes

1. U.S. Geological Survey programs 9208 CURVE and 9208 PEAKS written for this research by M. S. Hellman.
2. H. T. Evans, Jr., D. E. Appleman, D. S. Handwerker, Program, Am. Cryst. Assoc. meeting, Cambridge, Mass. (1963), p. 42.
3. G. Shirane, S. J. Pickart, R. Nathans, Y. Ishikawa, *J. Phys. Chem Solids* **10**, 35 (1959).
4. See R. W. Taylor, *Am. Mineral.* **49**, 1016 (1964); D. H. Lindsley, *Ann. Rept. Director Geophys. Lab.* **62**, 60 (1963); A. H. Webster and N. F. H. Bright, *J. Am. Ceram. Soc.* **44**, 110 (1961).
5. T. L. Wright and D. B. Stewart, *Am. Mineral.* **53**, 38 (1968).
6. F. Chayes, *Am. J. Science*, Bowen volume, 85 (1952).
7. J. V. Smith and P. Gay, *Mineral. Mag.* **31**, 744 (1958); H. -U. Nissen, in press.
8. We thank Mary E. Woodruff, U.S. Geological Survey, for assistance in mineral separation and data processing. Supported by NASA. Publication authorized by director, U.S. Geological Survey.

4 January 1970

Petrology of a Fine-Grained Igneous Rock from the Sea of Tranquillity

Abstract. *All phases in a thin section of sample 10022 have been analyzed by electron microprobe. Augite grains show strong iron enrichment in the outer 15 to 20 microns. Pigeonite cores occur within augite grains. The plagioclase has an anorthite content of between 73 and 81 mole percent and is high in Si and low in Al compared to stoichiometric feldspar. Residual phases include microcrystalline Fe-rich "pyroxene," plagioclase, K-rich alkali feldspar, silica, and rare areas rich in P and Zr with concentrations of Ba, Y, and rare earth elements. The density, viscosity, and crystallization history of the lava of sample 10022 are discussed.*

Results reported here are based primarily upon electron probe microanalyses (*1*) of a fine-grained vesicular igneous rock, NASA sample 10022,28. Phase designations are based principally on chemical composition and do not imply direct knowledge of structure. The rock has an igneous texture, and our interpretations assume that it crystallized from a melt. Average compositions of analyzed phases are presented in Tables 1 and 2. Volume percentages of the major phases have also been determined on the basis of 2000 random point identifications in transmitted and reflected light microscopy.

Skeletal ilmenite crystals up to several hundred microns long are distributed evenly throughout the section, some having delicate branches less than 10 μm wide. Euhedral ilmenite grains are enclosed in some augites; this suggests that ilmenite crystallized first. In section some ilmenite grains have rounded cavities filled with fine crystals of the other phases. The ilmenite exhibits no zoning or exsolution that can be resolved with the probe. Plagioclase crystals are often hollow and appear tubular in thin section, a habit characteristic of relatively rapid growth. The "tubes" are filled with an assortment of pyroxene, ilmenite, additional plagioclase, and residual phases. Plagioclase crystals occasionally transect the outer rims of augite. Many plagioclases grade into microcrystalline or glassy material of quartzofeldspathic composition. Figure 1a (detail) shows the range of composition in 19 plagioclase grains. There is not much systematic zoning of individual grains. In the average plagioclase of Table 2 Si $-$ (Na $+$ K) $=$ 2.10 and Al $-$ (Ca $+$ Fe $+$ Mg) $=$ 0.82 (based on eight oxygens), whereas these parameters are 2.00 and 1.00, respectively, in stoichiometric feldspars. Excess Si and a deficiency of Al have also been detected in terrestrial feldspars (*2*). The Ti and Fe (assumed to be Fe^{2+}) content is higher in the average lunar plagioclase of rock 10022 than in most terrestrial plagioclases.

Clinopyroxene is the most abundant phase and occurs in approximately equant grains up to several hundred microns in diameter. Most grains are composite, containing cores of pigeonite (10 to 100 μm) surrounded by augite. Pigeonite compositions (Fig. 1b) cluster close to the area where terrestrial pyroxene trends show inversion from orthopyroxene to pigeonite. There is a sharp composition break between the pigeonite and augite (Fig. 1, b and c). In contrast to the lack of zoning in the pigeonite, there is a continuous increase of Ca relative to Mg in the main body of the augite, followed by a sharp increase of Fe and a decrease of Mg and Ca in the outer 20 μm. The minor elements Ti, Al, and Cr are enriched in augite relative to pigeonite whereas Mn shows a reversed distribution. Titanium, Al, and Cr decrease in the augite rims whereas Mn increases. The smooth composition trends in the main body of the augites are similar to trends observed in plutonic terrestrial pyroxenes and may reflect growth from an ample liquid reservoir under near equilibrium conditions, whereas the abrupt zoning of the rims may be due to rapid changes of local residual liquid composition. Some augite rims appear to grade into material of Fe-rich pyroxene composition associated with other residual phases. The profile labeled *ar-rp* (Fig. 1b) extends from an augite rim into such a residual phase area. X-ray area scans across pigeonite-augite boundaries often reveal irregular borders suggestive of resorption of pigeonite and compatible with a peritectic reaction between pigeonite, augite, and liquid. Several grains of olivine (10 to 20 μm) are included in augite crystals. It seems likely that minor olivine crystallized before augite. Troilite is present as small interstitial blebs 5 to 30 μm in diameter. Its composition is close to that of stoichiometric FeS, and it has a lower content of Ti than some chondritic troilites have, in spite of the high Ti content of the rock. This may be related to conditions that contribute to a greater amount of oxidation or to the late crystallization of troilite after most of the Ti had been incorporated into ilmenite. Subspherical grains of iron ($\leqslant 5$ μm) are enclosed in some troilites with a texture suggestive of immiscible liquids. The Ni content of the iron averages 0.9 percent by weight with a maximum content of 1.4 percent observed.

As magma crystallization proceeded to the final stages, it was probable that certain constituents of the melt would solidify in phases other than the major phases described above. In terrestrial lavas it is usual to find residual constituents in the form of glass plus fine-grained matrix minerals. We have not identified glass, but a systematic search for residual phases has revealed patches of interstitial material which we interpret to be the crystallization product of a highly differentiated last-stage liquid. The overall average composition of this interstitial material is given in Tables 1 and 2; the analysis was also calculated in terms of normative components, and the results show the composition to be quite siliceous. The residual material is further resolved by probe analysis into the following fractions: (i) Areas of Fe-rich pyroxene composition, often adjacent to augites. Analyses of such areas are plotted as triangular symbols in Fig. 1b, and the average is given in Tables 1 and 2. Some of these "pyroxene" compositions are thought to be unstable in the pyroxene structure at low pressures (*3*). Within the resolution of the probe, these areas represent a homogeneous phase, but they may not have true pyroxene structure. (ii) Nearly pure silica, believed to be a primary igneous phase crystallized from a silica-saturated residual melt strongly differentiated from the initial ultrabasic

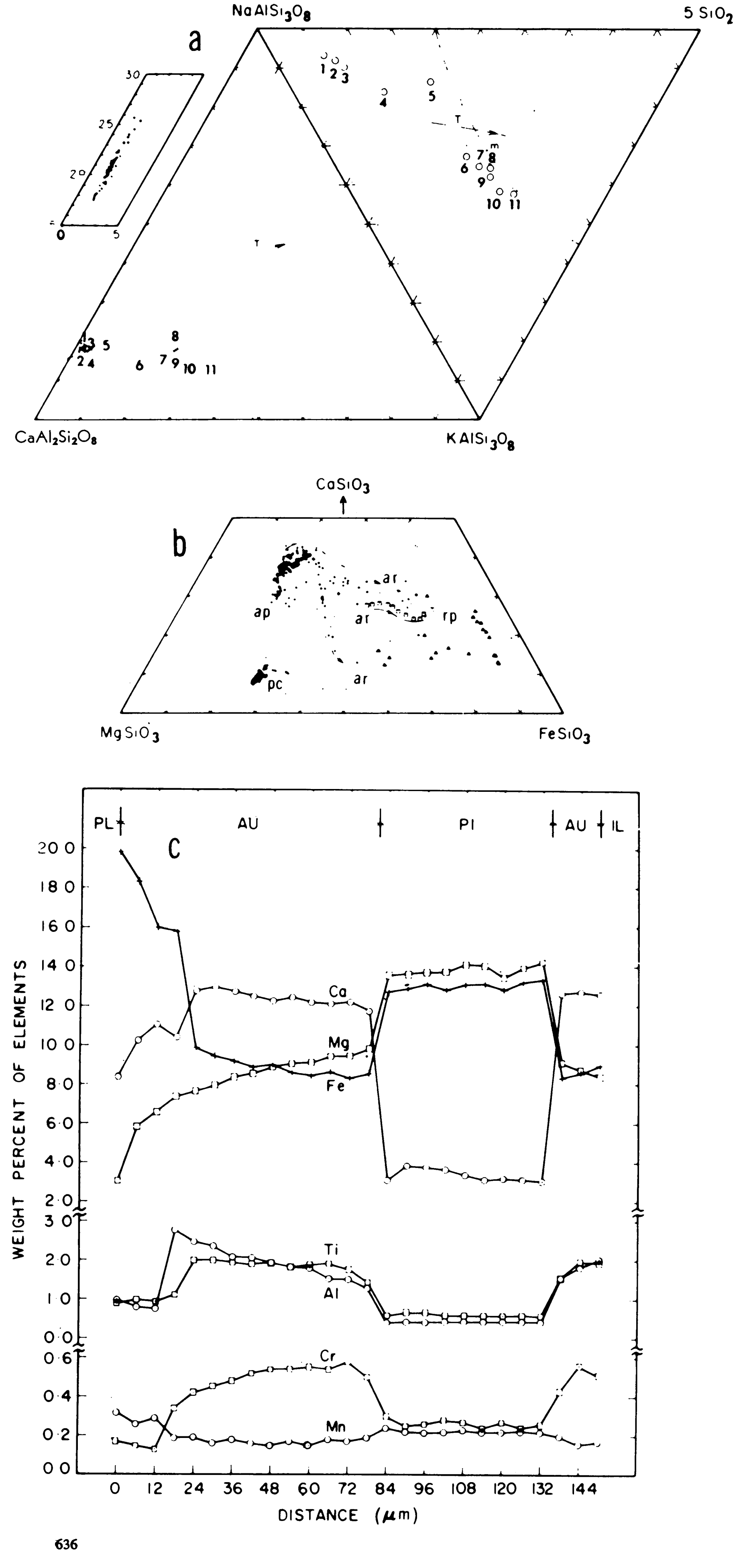

Fig. 1. Plagioclase, pyroxene, and residual phase compositions. (a) Small filled circles (detail) represent the results of 48 plagioclase analyses; Nos. 1 through 11 represent a profile from a plagioclase grain through a residual material of quartzo-feldspathic composition (anorthite + albite + orthoclase + quartz $\geqslant$ 88 percent by weight of total); *T* = Tasmanian dolerite salic trend (*4*); *m* = albite-orthoclase-quartz minimum at a water pressure of 500 kg/cm². (b) Pigeonite cores, *pc;* profiles from augite-pigeonite boundary to augite rim, *ap-ar;* profile from augite rim through residual "pyroxene," *ar-rp;* residual "pyroxene" analyses, triangles. (c) Profile across composite pyroxene; *PL,* plagioclase; *AU,* augite; *PI,* pigeonite; *IL,* ilmenite.

Table 1. Average compositions of phases in sample 10022 by electron probe microanalysis. Totals are given as oxides except for troilite and iron. Assumed oxidation states of elements are shown.

Phase	No. of spots-No. of grains	Elements (percentage by weight)												Totals
		Si^{4+}	Ti^{4+}	Al^{3+}	Cr^{3+}	Fe^{2+}	Mg^{2+}	Ca^{2+}	Mn^{2+}	Ni^{2+}	Na^{+}	K^{+}	S^{2-}	
Ilmenite	30-9	0.16	31.9		0.37	35.6	0.75	0.21	0.28					101.78
Olivine	7-2	17.2	0.19	0.10	0.15	22.1	20.3	0.35	0.23					100.47
Pigeonite	54-7	24.7	0.61	0.50	0.28	13.2	13.8	3.33	0.23		0.017			100.05
Augite	149-12	22.7	1.68	1.83	0.43	11.2	8.22	11.6	0.20		0.07			100.10
Plagioclase	30-19	23.8	0.10	16.0		0.66	0.20	10.9			1.75	0.21		100.39
Troilite	14-11	0.20	0.33		0.03	63.2		0.22		0.02			36.1	100.53
Iron	5-5	0.21	0.32		0.02	97.1			0.02	0.89			0.17	98.73
Residual														
Average	114-5	27.5	0.44	9.04	0.03	6.81	0.80	6.92	0.08		0.86	1.62		99.94*
"Pyroxene"	20-4	21.3	0.85	0.86	0.07	29.8	2.54	5.88	0.41		0.01			100.10
Silica	12-4	46.7	0.19	0.35	0.01	0.43	0.08	0.08			0.04			101.69
P-rich area	1-1	11.5	0.23	1.7		6.1	0.24	22.1			0.13	0.64		99.27†

*Includes 0.25 percent by weight BaO. †See text for additional elements which are included in total.

liquid. (iii) Rare areas rich in P and Zr which are associated with notable enrichment in exotic elements. In Table 1 we list the results of an analysis of an area rich in P which contains in addition to 9.9 percent by weight P (in percentage by weight): Y = 1.5, Ba = 0.22, La = 0.54, Ce = 1.4, Pr = 0.37, Nd = 1.5, Sm = 0.42, Gd = 0.57, Dy = 0.48, plus detectable amounts of Cl. Separate Zr concentrations (up to 18 percent by weight) with detectable amounts of Y, Ba, La, and Ce (but no P) have also been found in the residual material. We interpret these occurrences to be due to microcrystalline apatite and possibly zircon only partially resolved with the probe. (iv) Patches resembling eutectic microstructures often gradational with plagioclase grains. The average composition of these areas is represented by the salic portion of the formula for the average residual material in Table 2. A profile (4-μm steps) starting at the edge of a plagioclase grain and extending into this salic residue is illustrated in Fig. 1a (Nos. 1 through 11). The trend shows strong K and Si enrichment outward from the plagioclase, thus reflecting the progressive differentiation of the residual liquid. In Fig. 1a these residual liquid trends may be compared to those observed in the salic constituents of a Tasmanian dolerite (*4*). In both cases the trend, projected from the anorthite apex, approaches the ternary minimum in the albite-orthoclase-quartz system. While the terrestrial trend is defined by the salic constituents of a large differentiated complex, we are here dealing with several microns in one thin section. Although the microstructure is too fine to be completely resolved with the probe ($\leqslant$2 to 3 μm), it is possible with a small probe to partially resolve it into Ca-, K-, and Si-rich areas, which we interpret to be microcrystalline intergrowths of plagioclase, alkali feldspar, and silica, that is, microgranodiorite. Whether comparable igneous differentiation occurred on a larger scale on the moon remains to be seen.

Experimental work on a synthetic equivalent [11 major elements as given in (*5*)] of sample 10022 has been carried out in an Ar-atmosphere furnace with iron filings in the hot zone as an oxygen getter. Results given here are for runs held for 10 hours at the desired temperature, followed by quenching to 0°C in less than 2 seconds. Analyses of quench products are made by microprobe, x-ray diffraction, and microscopy. Ilmenite crystallizes at a liquidus temperature of 1300° ± 25°C, and there is an interval of approximately 100°C before pyroxene begins to crystallize. Plagioclase crystallizes at a somewhat lower temperature than pyroxene but is not equilibrated with the liquid in 10 hours, as indicated by a wide range of compositions. The equilibrium partition of Si, Al, Na, and Ca between plagioclase and liquid has been developed into a geothermometer (*6*). We have considered the temperatures at which the average plagioclase [An_{79} (79 mole percent anorthite)] would equilibrate with liquids from sample 10022 remaining after all of the ilmenite (21 percent by weight) and pigeonite (5 percent by weight), and varying amounts of augite, have been removed. Accordingly, the beginning of plagioclase crystallization is calculated to have occurred at between 1075° and 1175°C, corresponding to prior crystallization of 0 to 40 percent by weight augite. Experimental and theoretical arguments thus lead to a general view of the crystallization of sample 10022

Table 2. Average chemical formulas of phases in sample 10022.

Phase	Formula	Percentage by volume	Density (g/cm³)	Percentage by weight
Ilmenite	$(Fe_{7.54}Mg_{.37}Ca_{.06}Mn_{.06})_{8.03}(Ti_{7.86}Cr_{.08}Si_{.07})_{8.01}O_{24}$	15	4.8	21
Olivine	$(Mg_{1.34}Fe_{.64}Ca_{.014}Mn_{.0066}Cr_{.0047})_{2.01}(Si_{.986}Al_{.006}Ti_{.006})_{.998}O_{4}$			
Pigeonite	$(Fe_{2.09}Mg_{5.02}Ca_{.74}Mn_{.037}Na_{.0065}Cr_{.048}Al_{.060})_{8.00}(Si_{7.78}Al_{.10}Ti_{.11})_{7.99}O_{24}$	5	3.4	5
Augite	$(Fe_{1.82}Mg_{3.08}Ca_{2.64}Mn_{.033}Na_{.028}Cr_{.075}Al_{.29})_{7.97}(Si_{7.36}Al_{.33}Ti_{.32})_{8.01}O_{24}$	50	3.4	50
Plagioclase	$(Ca_{.744}Na_{.208}K_{.014}Fe_{.032}Mg_{.022})_{1.020}(Si_{2.32}Al_{1.62}Ti_{.0059})_{3.95}O_{8}$	29	2.7	23
Troilite	$(Fe_{1.00}Ti_{.007}Si_{.007}Ca_{.005})_{1.02}S$	1*	4.8	1
Iron	$Fe_{.997}Ni_{.0091}S_{.0025}Ti_{.0059}Cr_{.0003}Mn_{.0001}Si_{.0051}$			
Residual				
Average †	$23.5(Wo_{23}Fs_{60}En_{16}Rh_{1}) + 59.7(Or_{20}Ab_{18}An_{61}Cn_{1}) + 16.3\ SiO_2 + 0.5\ TiO_2$			
"Pyroxene"	$(Fe_{5.36}Mg_{1.04}Ca_{1.47}Mn_{.075}Na_{.0044}Cr_{.01}Al_{.16})_{8.12}(Si_{7.62}Al_{.16}Ti_{.18})_{7.96}O_{24}$			
Silica	$(Si_{11.9}Al_{.091}Cr_{.002}Fe_{.054}Ca_{.013}Mg_{.023}Ti_{.028}Na_{.01})_{12.1}O_{24}$			

*Includes iron and all others. † Formula based on one cation per pyroxene and feldspar molecule.

which confirms the textural relations.

The density and logarithm of viscosity of silicate melts are approximately linear functions of composition, and published density and viscosity data for simple silicate systems allow one to calculate these properties for natural lavas with accuracies comparable to those of current measurements (*7*). We calculate the density of sample 10022 liquid to be 2.93 to 2.96 g/cm^3 between 1400° and 1250°C. The viscosity varies from 6 to 27 poises over the same temperature range, which is comparable to the viscosity of glycerin at room temperature. The low viscosity [the viscosities of olivine basalts (*8*) range at least an order of magnitude higher] is related to low concentrations of Si and Al and makes it likely that, for comparable thermal histories, lunar lavas, in spite of lower gravity, are capable of faster and more extensive flow than their terrestrial counterparts. In view of the large areal extent of plateau-type lavas on earth, it is not difficult to imagine lunar lavas flowing, topography permitting, over areas comparable to mare basins. The pronounced fluidity might also result in the formation of long lava tubes which could form sinuous rills when the upper crusts are breached. The large density contrast between ilmenite and the liquid, the long ilmenite crystallization interval, and the low viscosity of the liquid would favor ilmenite-liquid separation wherever lavas were ponded to any depth. The igneous rocks of the Sea of Tranquillity may owe their high ilmenite content to such a mechanism, and mascons may be related to concentrations of dense, early-crystallizing solids in the central portions of the basins of the deeper circular maria. In any case, such reasoning leads one to expect that the ilmenite (and therefore Fe and Ti) content may be quite variable over the lunar surface.

DANIEL F. WEILL
I. STEWART MCCALLUM, YAN BOTTINGA
MICHAEL J. DRAKE, GORDON A. MCKAY
Center for Volcanology, University of Oregon, Eugene 97403

References and Notes

1. Standard analytical conditions: Applied Research Labs electron microprobe x-ray analyzer; 15 kv; sample current, 30 to 50 × 10^{-9} amperes; 1- to 2-μm beam; 10-second counting interval. When convenient, Ti through Ni were analyzed at 20 kv. The counting interval was increased for minor elements, and a larger beam was used in alkali-rich areas. Drift, dead time, background, absorption, generation, and fluorescence corrections were applied to all analyses. Details of all analyses are available on request.
2. K. Perry, Jr., *Lithos* **1**, 201 (1968).
3. D. H. Lindsley and J. L. Munoz, *Amer. J. Sci.* **267-A**, 295 (1969).
4. I. McDougall, *Bull. Geol. Soc. Amer.* **73**, 279 (1962). Salic trends are taken from the interpretation by I. S. E. Carmichael, *Quart. J. Geol. Soc. London* **119**, 95 (1963).
5. Lunar Sample Preliminary Examination Team, *Science* **165**, 1211 (1969).
6. A. M. Kudo and D. F. Weill, *Contrib. Mineral. Petrol.*, in press.
7. Y. Bottinga and D. F. Weill, abstract, *Trans. Amer. Geophys. Union* **50**, 676 (1969); in preparation.
8. Kani, *Proc. Imp. Acad. Tokyo* **10**, 29, 79 (1934).
9. We thank R. Freeman, H. Howard, and E. Oas for technical assistance. Supported by NASA contract NAS 9-8071 and NASA grant NGR 38-003-009.

4 January 1970

High-Voltage Transmission Electron Microscopy Study of Lunar Surface Material

Abstract. *The internal substructures of a type B sample have been examined at high magnification and compared with terrestrial rocks. Selected ultrathin sections were prepared from these multiphase materials by an ion-thinning technique and examined in a 1-Mev electron microscope, with complementary optical analyses. The structures in the ilmenite and plagioclase indicate that the lunar material has undergone plastic deformation by dislocation movement and possibly microtwinning, with subsequent recovery. The pyroxene exhibits complex lamellar structures of submicron spacing. These various observations are consistent with the optical microscopy evidence for distortion and recovery and identify the processes involved.*

The use of transmission electron microscopy to study the fine-scale substructure in thin foils of metals and some ceramic materials during the past decade has been of considerable value in elucidating various structure-history and structure-property relationships (*1*). However, with few exceptions, this technique has not been applied to geological materials because of the difficulty of preparing suitable electron-transparent foils from multiphase nonmetallic solids. Previous electron microscopy studies of geological importance appear to have been restricted to a few single-phase rock-forming minerals (*2*, *3*), with thin foils usually prepared by mechanical cleavage. The latter method has the major disadvantages of uncertainty as to the location of the fragment in the original specimen and the possibility of introducing artifacts.

Although the potential of ion-bombardment thinning to prepare foils for electron microscopy was recognized some 20 years ago (*4*), only recently has apparatus capable of producing glow-discharge plasma beams that are stable over long periods of time been perfected (*5*). Such apparatus can successfully thin metals and ceramics and has now been shown to be suitable for a number of geologically important materials (*6*). However, the foil thickness of a few thousand angstroms required for conventional (100-kv) transmission microscopy results in a delicate and friable specimen which is easily broken and destroyed in handling. Consequently, the recent advent of high-voltage microscopy offers a major advantage for the study of geological materials because the specimen thickness can be increased to the order of 1 μm, which facilitates both preparation and handling. Furthermore, the higher voltage permits increased resolution by reduction of chromatic aberration, increased precision of selected-area electron diffraction, and reduction of the possibility of specimen damage in the microscope from ionization and beam heating effects.

The combination of ion thinning and high-voltage microscopy has particular value for the study of the substructure of lunar material, in that wastage and loss during specimen preparation of the limited amount of available material is minimized. The present paper describes the application of these new techniques to the study of the substructure of a sample of type B lunar rock (Preliminary Examination Team Report sample 10029-1) with the objectives of comparing the principal characteristics with those of analogous terrestrial material to assist in elucidating the mechanical and thermal history of the lunar material. This study is the first in a program of electron microscopy observations of the internal structure of lunar surface material brought back from the Apollo 11 and 12 missions.

The specific techniques used for preparing and examining the 10029-1 sample were developed on specimens of terrestrial rocks chosen to simulate the lunar material as closely as possible. The initial series of simulation specimens included several Hawaiian basalts, together with pyroxenite and anorthosite. After the release of chemical analyses and